Acta Cryst. (1965). **18**, 282

The Diffraction Pattern of Fine Particle Carbon Blacks*

BY B. E. WARREN AND P. BODENSTEIN

Massachusetts Institute of Technology, Cambridge, Massachusetts, U.S.A.

(*Received* 18 *March* 1964)

The diffraction patterns of fine particle turbostratic carbons have been obtained from the general Debye scattering equation. Diamond's treatment for a single layer has been extended to include the interaction between the different layers in a parallel layer group. The method leads to theoretical diffraction patterns from which quantities such as peak positions, peak areas above background, and peak breadths can be obtained rigorously.

Introduction

The finely divided carbon blacks are a turbostratic form of carbon in which parallel graphite layers have random orientations about the layer normal. The X-ray diffraction pattern from such a material shows only the three-dimensional lattice reflections $00l$ and the two-dimensional lattice reflections hk. The parallel layer group dimension normal to the layers is called L_c, and its value is usually obtained from a measurement of the half maximum intensity breadth B of the 002 reflection and calculation from the Scherrer equation.

$$L_c = 0{\cdot}94\lambda/B\cos\theta\,. \tag{1}$$

The layer dimension L_a is obtained from the half maximum intensity breadth of an hk reflection and the two-dimensional lattice equation (Warren, 1941).

$$L_a = 1{\cdot}84\lambda/B\cos\theta\,. \tag{2}$$

For the larger sized blacks ($L_a > 50$ Å), equation (2) gives a satisfactory representation. However, the approximations involved in the derivation are such that, for the smaller blacks, the values obtained are progressively more unreliable the smaller the black. To obtain a better representation for the smaller sized blacks, Diamond (1957) evaluated the powder pattern for the case of a single layer by using the general Debye scattering equation

$$I(s) = \sum_m \sum_n f_m f_n \frac{\sin 2\pi s r_{mn}}{2\pi s r_{mn}} \tag{3}$$

where $s = 2\sin\theta/\lambda$, and r_{mn} is the distance between atoms m and n. For a sample containing only single layers, the values tabulated by Diamond give a rigorous representation of the hk peaks. However, for samples in which there are parallel layer groups containing several layers, there will also be $00l$ reflections, and additional modulations which affect the shape of the hk reflections. To have a rigorous representation of features such as peak breadths and peak displacements, and for purposes of discussing the fraction of disorganized carbon to have accurate intensity minima and peak areas above apparent background levels, it is desirable to extend Diamond's treatment to include the case of parallel layer groups containing several layers. It is only necessary to add the interaction between layers, and since the layers have random orientation about the layer normal, each layer can be represented by a uniform distribution of atoms, and the sums replaced by simple integrals.

* Research sponsored by the U.S. Atomic Energy Commission.

Scattering by a parallel-layer group

We assume disk-shaped graphite layers of radius R and separation z. Let M be the number of layers in a parallel layer group, and N the number of atoms in a single layer. The sum over all the atoms can be expressed in terms of a sum over layers p and over atoms within a layer m. For one parallel-layer group, the intensity in electron units is given by

$$I_{eu} = \sum_p \sum_m \sum_{m'} f^2 \frac{\sin 2\pi s r_{mm'}}{2\pi s r_{mm'}} + \sum_p \sum_{p' \neq p} \sum_m \sum_{m'} f^2 \frac{\sin 2\pi s r_{mm'}}{2\pi s r_{mm'}}\,. \tag{4}$$

Let $q = p - p'$, and introduce the abbreviation

$$i(q) = \frac{1}{N} \sum_m \sum_{m'} \frac{\sin 2\pi s r_{mm'}}{2\pi s r_{mm'}}\,. \tag{5}$$

The intensity is then expressed by the simple sum

$$I_{eu}/MNf^2 = i(0) + (1 - 1/M)2i(1) + (1 - 2/M)2i(2) + \ldots . \tag{6}$$

The quantity $i(0)$ has been computed and tabulated by Diamond, and it now remains to evaluate $i(q)$ for $q \neq 0$.

For q not equal to zero, the sum in equation (5) can be replaced by an integral

$$i(q) = \frac{1}{N} \iint \frac{\sin 2\pi s r}{2\pi s r} \frac{N dA}{\pi R^2} \frac{N dA'}{\pi R^2} \tag{7}$$

where dA and dA' are elements of area in the two layers with separation qz, and r is the distance between dA and dA'. It is convenient to express equation (7) in the form

$$i(q) = \frac{N}{\pi^2 R^4} \int \frac{\sin 2\pi sr}{2\pi sr} \left[\int dA dA' \right]_r \qquad (8)$$

where the term in square brackets means an integral over both layers of all elements of area dA and dA' with separations between r and $r+dr$. Let h be the horizontal projection of r, so that

$$r^2 = h^2 + (qz)^2. \qquad (9)$$

Elements of area dA and dA' at constant separation r will be at constant projected separation h.

In Fig. 1 the element of area dA in one layer has an element $dA' = 2\beta h dh$ in the other layer at the projected distance h. The value of dA' is the same if dA is any part of the ring-shaped area $2\pi x dx$, and hence

$$\left[\int dA\, dA' \right]_r = \left[\int 2\pi x dx 2\beta h dh \right]_h = 2\pi h dh \left[\int 2\beta x dx \right]_h .$$

The area $2\beta x dx$ is shown on Fig. 1 by the cross-hatched area $2\beta' x dx$ where $\beta' = \beta$. From the equivalence of the triangles $OdAC$ and $OO'D$, it is evident that

$$\left[\int 2\beta' x dx \right]_h = S$$

where S is the overlap area of two disks of radius R with centers separated by the distance h. With the abbreviation $u = h/2R$, the overlap area is given by

$$S = 2R^2 \{ \text{arc cos } u - u(1-u^2)^{\frac{1}{2}} \} .$$

Table 1. *Values of* $i(q)$

	$z = 3{\cdot}44$ Å		$2R = 20$ Å		$z = 3{\cdot}44$ Å		$2R = 30$ Å	
s	$i(1)$	$i(2)$	$i(3)$	$i(4)$	$i(1)$	$i(2)$	$i(3)$	$i(4)$
0·06	6·807	−9·926	−14·041	−1·755	7·237	−9·979	−11·792	3·050
0·07	2·369	−10·052	−5·413	7·780	2·319	−10·497	−4·421	8·544
0·08	0·409	−7·728	1·484	7·690	−0·489	−8·546	1·963	7·369
0·09	−0·935	−5·241	4·573	2·386	−1·648	−5·413	5·354	2·048
0·10	−2·085	−3·023	4·730	−2·309	−2·528	−2·760	5·232	−2·925
0·11	−2·816	−0·940	3·313	−3·804	−3·100	−0·535	3·353	−4·249
0·12	−3·018	0·873	1·215	−2·557	−3·140	1·296	0·936	−2·569
0·13	−2·881	2·072	−0·850	−0·172	−3·015	2·315	−1·285	0·139
0·14	−2·655	2·503	−2·165	1·756	−2·863	2·599	−2·445	2·156
0·15	−2·429	2·325	−2·321	2·187	−2·547	2·443	−2·344	2·315
0·16	−2·154	1·811	−1·499	1·096	−2·145	1·898	−1·449	0·911
0·17	−1·791	1·144	−0·289	−0·528	−1·778	1·094	−0·220	−0·726
0·18	−1·380	0·416	0·737	−1·474	−1·395	0·297	0·881	−1·562
0·19	−0·993	−0·277	1·273	−1·241	−0·988	−0·380	1·415	−1·261
0·20	−0·660	−0·809	1·255	−0·244	−0·632	−0·893	1·303	−0·176
0·21	−0·363	−1·086	0·781	0·709	−0·321	−1·153	0·744	0·833
0·22	−0·082	−1·108	0·073	1·037	−0·028	−1·151	−0·008	1·109
0·23	0·170	−0·937	−0·564	0·652	0·215	−0·964	−0·647	0·652
0·24	0·369	−0·644	−0·880	−0·099	0·396	−0·641	−0·927	−0·182
0·25	0·507	−0·285	−0·798	−0·689	0·540	−0·243	−0·811	−0·767
0·26	0·598	0·083	−0·423	−0·742	0·643	0·135	−0·413	−0·755
0·27	0·658	0·391	0·051	−0·287	0·691	0·429	0·094	−0·245
0·28	0·684	0·584	0·440	0·302	0·703	0·616	0·500	0·349
0·29	0·673	0·641	0·617	0·606	0·687	0·671	0·653	0·641
0·30	0·625	0·579	0·538	0·466	0·637	0·595	0·539	0·473
0·31	0·552	0·429	0·255	0·039	0·561	0·427	0·236	0·006
0·32	0·468	0·223	−0·097	−0·361	0·474	0·208	−0·128	−0·406
0·33	0·376	−0·003	−0·369	−0·479	0·374	−0·028	−0·399	−0·499
0·34	0·274	−0·207	−0·463	−0·266	0·264	−0·232	−0·482	−0·253
0·35	0·167	−0·350	−0·368	0·105	0·158	−0·368	−0·373	0·138
0·36	0·063	−0·412	−0·144	0·370	0·056	−0·429	−0·132	0·396
0·37	−0·029	−0·395	0·112	0·357	−0·040	−0·408	0·139	0·360
0·38	−0·109	−0·312	0·303	0·103	−0·124	−0·314	0·326	0·088
0·39	−0·178	−0·184	0·358	−0·193	−0·192	−0·175	0·368	−0·215
0·40	−0·234	−0·033	0·266	−0·329	−0·246	−0·020	0·265	−0·347
0·41	−0·275	0·111	0·077	−0·232	−0·285	0·126	0·067	−0·233
0·42	−0·297	0·222	−0·123	0·010	−0·305	0·236	−0·140	0·029
0·43	−0·302	0·281	−0·256	0·226	−0·310	0·293	−0·272	0·246
0·44	−0·294	0·285	−0·278	0·272	−0·301	0·294	−0·287	0·279
0·45	−0·275	0·240	−0·191	0·130	−0·279	0·243	−0·190	0·122
0·46	−0·244	0·156	−0·036	−0·090	−0·245	0·152	−0·025	−0·106
0·47	−0·204	0·051	0·121	−0·231	−0·204	0·042	0·136	−0·243
0·48	−0·157	−0·057	0·219	−0·202	−0·156	−0·066	0·229	−0·204
0·49	−0·107	−0·145	0·222	−0·040	−0·105	−0·154	0·226	−0·031
0·50	−0·057	−0·200	0·137	0·136	−0·053	−0·209	0·136	0·150

Table 1 (*cont.*)

	$z=3{\cdot}44$ Å		$2R=20$ Å		$z=3{\cdot}44$ Å		$2R=30$ Å	
s	$i(1)$	$i(2)$	$i(3)$	$i(4)$	$i(1)$	$i(2)$	$i(3)$	$i(4)$
0·51	−0·009	−0·214	0·006	0·207	−0·003	−0·221	−0·002	0·216
0·52	0·038	−0·190	−0·118	0·133	0·044	−0·193	−0·129	0·130
0·53	0·080	−0·135	−0·186	−0·026	0·085	−0·133	−0·195	−0·037
0·54	0·114	−0·059	−0·178	−0·157	0·119	−0·054	−0·181	−0·167
0·55	0·140	0·024	−0·099	−0·172	0·146	0·030	−0·096	−0·175
0·56	0·158	0·096	0·013	−0·068	0·164	0·102	0·021	−0·063
0·57	0·169	0·145	0·113	0·075	0·173	0·151	0·121	0·084
0·58	0·171	0·165	0·161	0·157	0·173	0·171	0·167	0·164
0·59	0·164	0·155	0·142	0·127	0·167	0·157	0·145	0·127
0·60	0·150	0·118	0·069	0·012	0·152	0·117	0·066	0·006
0·61	0·131	0·062	−0·027	−0·103	0·131	0·059	−0·033	−0·112
0·62	0·107	−0·002	−0·106	−0·141	0·107	−0·007	−0·113	−0·146
0·63	0·080	−0·062	−0·139	−0·081	0·078	−0·067	−0·144	−0·079
0·64	0·050	−0·107	−0·115	0·031	0·048	−0·111	−0·116	0·038
0·65	0·019	−0·129	−0·047	0·116	0·017	−0·133	−0·044	0·122
0·66	−0·010	−0·127	0·036	0·116	−0·012	−0·130	0·042	0·118
0·67	−0·037	−0·103	0·100	0·037	−0·040	−0·104	0·105	0·033
0·68	−0·060	−0·062	0·120	−0·063	−0·064	−0·060	0·124	−0·069
0·69	−0·080	−0·011	0·092	−0·114	−0·083	−0·088	0·092	−0·118
0·70	−0·095	0·039	0·029	−0·084	−0·098	0·042	0·026	−0·084
0·71	−0·105	0·078	−0·042	0·001	−0·108	0·082	−0·047	0·006
0·72	−0·109	0·102	−0·093	0·081	−0·111	0·105	−0·097	0·087
0·73	−0·108	0·106	−0·104	0·102	−0·110	0·108	−0·107	0·104
0·74	−0·103	0·091	−0·073	0·051	−0·104	0·092	−0·073	0·049
0·75	−0·093	0·060	−0·015	−0·032	−0·093	0·059	−0·012	−0·037
0·76	−0·079	0·020	0·046	−0·089	−0·079	0·018	0·050	−0·093
0·77	−0·062	−0·022	0·086	−0·082	−0·062	−0·024	0·089	−0·083
0·78	−0·043	−0·057	0·090	−0·019	−0·042	−0·060	0·092	−0·016
0·79	−0·023	−0·081	0·058	0·054	−0·022	−0·084	0·057	0·058
0·80	−0·003	−0·089	0·004	0·086	−0·002	−0·091	0·002	0·089
0·81	0·016	−0·080	−0·048	0·058	0·017	−0·081	−0·052	0·058
0·82	0·033	−0·058	−0·079	−0·009	0·035	−0·057	−0·082	−0·012
0·83	0·049	−0·026	−0·077	−0·067	0·050	−0·025	−0·078	−0·070
0·84	0·061	0·009	−0·044	−0·076	0·062	0·011	−0·044	−0·077
0·85	0·069	0·041	0·004	−0·033	0·071	0·044	0·007	−0·031
0·86	0·075	0·064	0·049	0·031	0·076	0·066	0·052	0·034
0·87	0·076	0·074	0·072	0·071	0·078	0·076	0·075	0·073
0·88	0·075	0·071	0·066	0·060	0·075	0·072	0·067	0·060
0·89	0·069	0·055	0·034	0·008	0·070	0·055	0·033	0·006
0·90	0·061	0·029	−0·011	−0·046	0·061	0·029	−0·013	−0·050
0·91	0·050	0·000	−0·049	−0·067	0·050	−0·002	−0·052	−0·069
0·92	0·038	−0·028	−0·066	−0·041	0·037	−0·030	−0·068	−0·040
0·93	0·024	−0·050	−0·056	0·013	0·023	−0·052	−0·057	0·015
0·94	0·010	−0·062	−0·024	0·055	0·009	−0·064	−0·023	0·058
0·95	−0·004	−0·062	0·016	0·058	−0·005	−0·064	0·018	0·059

From equation (9) it follows that $h\,dh = r\,dr$ and hence

$$\left[\int dA\,dA'\right]_r = 4\pi R^2 \{\arccos u - u(1-u^2)^{\frac{1}{2}}\} r\,dr\,. \quad (10)$$

Assuming an axial length $a=2{\cdot}461$ Å for the cell containing two atoms, the area per atom is $\pi R^2/N = 2{\cdot}624$ Å^2. Combining equations (8) and (10), we obtain finally

$$i(q) = \frac{0{\cdot}2427}{s}\int_{r=qz}^{r=r_m} \{\arccos u - u(1-u^2)^{\frac{1}{2}}\} \sin 2\pi s r\,dr \quad (11)$$

where $r_m = [(2R)^2 + (qz)^2]^{\frac{1}{2}}$.

Equation (11) represents a Fourier transform which is readily programmed for machine computation to give $i(q)$ as a function of s for various integral values of q, layer diameters $2R$, and layer separation z. The values listed in Table 1 are computed for a layer separation $z=3{\cdot}44$ Å, and diameters $2R=20$ Å and $2R = 30$ Å. For the larger values of s, the values of $i(q)$ are well enough approximated by $i(q) = (0{\cdot}057/s^2)\cos 2\pi sqz$. Except for small values of s, the values of $i(q)$ do not depend strongly on R, and hence the values of Table 1 suffice for an intensity evaluation for any small particle carbon black with values of L_c up to $5\times 3{\cdot}44 = 17{\cdot}2$ Å.

Discussion

To have definite examples which can be compared with experiment, powder patterns have been evaluated for Cu $K\alpha$ ($\lambda=1{\cdot}542$ Å) and the two parallel-layer group sizes $L_c=13{\cdot}8$ Å, $L_a=20$ Å and $L_c=17{\cdot}2$ Å, $L_a=30$ Å. From equation (6), I_{eu}/MNf_c^2 is evaluated

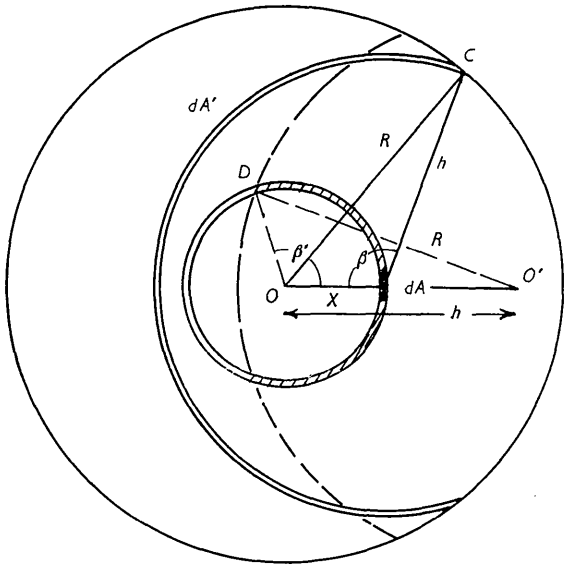

Fig. 1. Geometry involved in the distribution of neighbors with distance for two carbon layers of radius R.

as a function of s using $i(q)$ values for $2R=20$ Å and $2R=30$ Å from Table 1, and Diamond's $i(0)$ values for $L_a=20$ Å and $L_a=30$ Å. Each value of I_{eu}/MNf_c^2 was then multiplied by f_c^2, to this was added the intensity per atom of Compton modified scattering i_m, and the sum was then multiplied by the polarization factor so as to give curves comparable to that part of a powder pattern due to the parallel-layer groups. The final curves plotted against 2θ are shown in Figs. 2 and 3. The Compton modified scattering alone is shown by the dashed curves labelled CM. The oscillations which appear on either side of the 002 peak result from a calculation assuming only one L_c value. In the practical case, these oscillations are averaged out by a small range of L_c values,

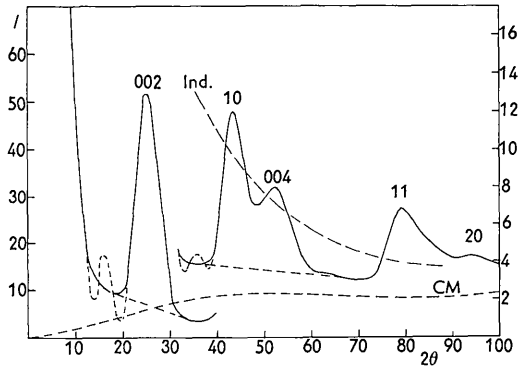

Fig. 2. Computed diffraction pattern for the parallel-layer group size $L_a=20$, $L_c=13{\cdot}8$ Å with radiation Cu $K\alpha$. For the solid curves the ordinate values are

$$(I_{eu}/MN+i_m)(1+\cos^2 2\theta)/2\,.$$

The dashed curves give the Compton modified and the independent unmodified plus modified scattering per atom.

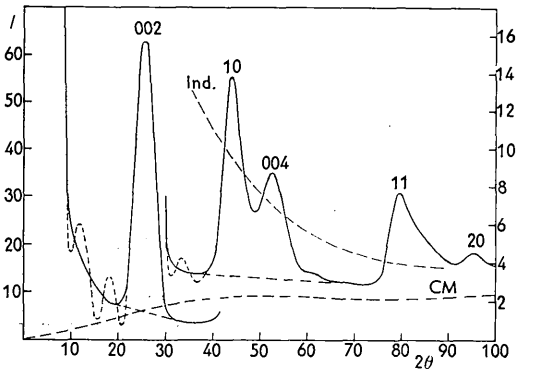

Fig. 3. Computed diffraction pattern for the parallel layer group size $L_a=30$, $L_c=17{\cdot}2$ Å with radiation Cu $K\alpha$. For the solid curves the ordinate values are

$$(I_{eu}/MN+i_m)(1+\cos^2 2\theta)/2\,.$$

The dashed curves give the Compton modified and the independent unmodified plus modlfied scattering per atom.

and hence an average intensity curve has been drawn through the oscillations.

The first striking point is that the minima between 002 and 10, and between 10–004 and 11, stand well above the Compton modified level. An appreciable part of the unmodified scattering from the parallel layer groups is not contained in the peak areas above a line drawn through consecutive minima. Allowance must be made for this in any attempt to evaluate the fraction of organized carbon in the sample, otherwise too low a fraction will be obtained.

By making the assumption that any additional background scattering in the vicinity of 10 and 004 is due only to disorganized carbon in which the carbon atoms scatter independently, it is possible to make an evaluation of the fraction of organized carbon from a pattern made with monochromatic Cu $K\alpha$ radiation. In the same units used in Figs. 2 and 3, the intensity per atom of independent scattering is given by $(f_c^2+i_m)(1+\cos^2 2\theta)/2$. The independent scattering curve is included in Figs. 2 and 3. Let A_1 be the area under the 10–004 peak above the line connecting minima. Let A_2 be the area below the line connecting minima and within the angular range $2\theta=40°$ to $2\theta=60°$. Let A_3 be the area under the independent scattering curve in the angular range $2\theta=40°$ to $2\theta=60°$. On the experimental curve let α be the ratio of the area of the 10–004 peak above the line connecting minima, to the area below the connecting line in the angular range $2\theta=40°$ to $2\theta=60°$. The fraction x of organized carbon (carbon contained in layer groups of one or more layers) is then given by

$$x=\frac{\alpha}{A_1/A_3+\alpha(1-A_2/A_3)}\,. \qquad (12)$$

For the sizes represented by Fig. 2, $A_1/A_3=0{\cdot}50$ and $A_2/A_3=0{\cdot}45$. From Fig. 3, the values are $A_1/A_3=0{\cdot}56$

and $A_2/A_3=0{\cdot}41$. Use of the area of the 002 peak would give the fraction of organized carbon in parallel layer groups containing two or more layers. However, it is not safe to compare the 002 peak area with a background in the vicinity of 002, since in this region there can be an appreciable contribution from small angle scattering. It is probably safer to compare the area of the 002 peak with the same diffuse area between $2\theta=40°$ and $2\theta=60°$ which has been used with the 10–004 peak.

It is sometimes of interest to check that a sample is free of preferred orientation. For this purpose it is convenient to use the ratio of the area of the 002 peak to the area of the combined 10–004 peak, in each case above the line connecting minima on either side. From Figs. 2 and 3, these ratios are $r=3{\cdot}11$ for $L_a=20$, $L_c=13{\cdot}8$ Å and $r=2{\cdot}92$ for $L_a=30$, $L_c=17{\cdot}2$ Å.

The data for Figs. 2 and 3 were computed with $d(002)=z=3{\cdot}44$ Å, and it is of interest to see how closely this value is reproduced from the position of the 002 peak. Applying the Bragg law to the midpoint of the 002 peak at three-quarters height, we obtain $d(002)=3{\cdot}54$ and $3{\cdot}52$ Å from Figs. 2 and 3. Correcting the 002 peak by dividing by $f_c^2(1+\cos^2 2\theta)/2$, we obtain $3{\cdot}47$ and $3{\cdot}45$ Å. In this case the discrepancy is less than the experimental uncertainty in locating the center of a broad peak. For a small particle carbon black, the 002 peak is usually superimposed on a rapidly dropping background, and it is important to make an approximate correction by subtracting a dropping background such that the reconstructed 002 peak has a new background of approximately equal height on either side.

The final question concerns how well the parallel layer group sizes can be obtained from the peak breadths. Application of equation (1) to the breadth of the 002 peak measured half way up from the line connecting minima, gives an L_c which is 8% greater than $4\times3{\cdot}44$ for Fig. 2, and 5% greater than $5\times3{\cdot}44$ for Fig. 3. This indicates that even for the very fine blacks, a fairly good value for L_c can be obtained directly from the 002 peak breadth without any correction for f_c^2 and the polarization factor. In practice it is preferable to subtract off a dropping background and make the measurement of breadth on the reconstructed 002 peak.

For obtaining the value of L_a from the breadths of the 10 and 11 peaks, there are additional difficulties. It might seem reasonable to make graphs of the 10 and 11 peaks for different values of L_a using Diamond's $i(0)$ values. By then measuring the breadth halfway up from the line connecting minima on either side, we can obtain the value of the factor K which should replace the number $1{\cdot}84$ in equation (2). The values obtained in this way are shown in Fig. 4. Although the values show an increase with L_a, they are well below the value $1{\cdot}84$ for the range of sizes considered here. There is a difference in the values of K for 10 and 11, and for $L_a<20$ Å the 11 breadths have little significance because they include a contribution from 20.

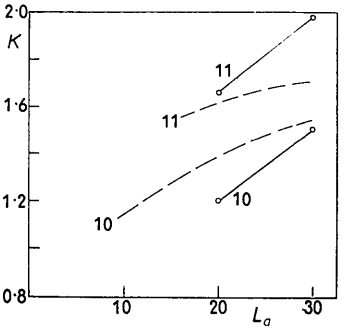

Fig. 4. Values of K to replace the number $1{\cdot}84$ in equation (2). The dashed curves are from Diamond's tabulated values for a single layer. The solid curves are from measurements on Figs. 2 and 3.

In the practical case we have parallel-layer groups containing more than one layer. Here there is the added complication that the 004 modulations give an additional narrowing of 10, and the 006 modulations give an additional broadening of 11. Values of the breadth halfway up from the line connecting minima on either side were measured on Figs. 2 and 3. The corresponding values of K for 10 and 11 are shown on Fig. 4. The breadths of the 10 and 11 peaks are influenced by the modulations which result from the other layers, and hence they depend to some extent on the L_c value for the sample.

If it is not necessary to obtain an accuracy in L_a values of better than 25%, it is probably good enough to make measurements of the breadth of 10 halfway up from the line connecting minima and choose an approximate value of K from Fig. 4. For more accurate values of L_a, where it may be desirable to allow for variations in L_c and for a range of sizes in L_a, it is probably desirable to make up a set of curves such as Figs. 2 and 3 covering a variety of L_a and L_c values.

This work was done in part at the Computation Center at the Massachusetts Institute of Technology, Cambridge. We are indebted to Dr A. I. Medalia and Dr F. A. Heckman of Cabot Corporation for discussions which suggested the need for this type of treatment. The contribution by one of us (P. B.) has been sponsored by the South African Atomic Energy Board.

References

DIAMOND, R. (1957). *Acta Cryst.* **10**, 359.
WARREN, B. E. (1941). *Phys. Rev.* **59**, 693.